SAND2016-5471C

# EXPERIMENTAL MEASUREMENT AND FINITE ELEMENT MODELING OF RESIDUAL STRESSES IN SIMPLE COMPOSITE STRUCTURES

Alexander A. Hanson[1], Stacy M. Nelson[1], Timothy M. Briggs[1], Brian T. Werner[1], Brent L. Volk[2], Tara Storage[2]

[1]Sandia National Laboratories
Livermore, CA 94551-0969

[2]Air Force Research Laboratory
WPAFB, OH 45433

## ABSTRACT

Process induced residual stresses commonly occur in composite structures composed of dissimilar materials. These residual stresses form due to differences in the composite materials' coefficients of thermal expansion as well as the shrinkage upon cure exhibited by most thermoset polymer matrix materials. Depending upon the specific geometric details of the composite structure and the materials' curing parameters, it is possible that these residual stresses can result in interlaminar delamination and fracture within the composite as well as plastic deformation in the structure's metallic materials. Therefore, the consideration of potential residual stresses is important when designing composite parts and their manufacturing processes. However, the experimental determination of residual stresses in prototype parts can be prohibitive, both in terms of financial and temporal costs. As an alternative to physical measurement, it is possible for computational tools to be used to quantify potential residual stresses in composite prototype parts. Therefore, the objective of this study is the development of a simplistic method for simulating the residual stresses formed in polymer matrix composite structures. Specifically, a simplified approach accounting for both coefficient of thermal expansion mismatch and polymer shrinkage is implemented within the Sandia National Laboratories' developed solid mechanics code, SIERRA. This approach is then used to model the manufacturing of two simple, bi-material structures composed of a carbon fiber/epoxy composite and aluminum: a flat rectangular plate and cylinders. Concurrent with the computational efforts, structures similar to those modeled are fabricated and the residual stresses are quantified through the measurement of deformation. The simulations' results are compared to the experimentally observed behaviors for model validation, as well as a more complex modeling approach. The results of the comparisons indicate that the proposed finite element modeling approach is capable of accurately simulating the formation of residual stresses in composite structures.

Sandia National Laboratories is a multi-program laboratory managed and operated by Sandia Corporation, a wholly owned subsidiary of Lockheed Martin Corporation, for the U.S. Department of Energy's National Nuclear Security Administration under contract DE-AC04-94AL85000

# 1. INTRODUCTION

Residual stresses in composite structures developed during the curing process, especially at the interface with another material, can lead to delamination or failure of the composite. Experiments can be done to determine the residual stress of a component; however, these are costly and difficult depending on the geometry of the component. As an alternative, validated computer simulations can be used to predict the residual stress and subsequent failure of a component. This represents a potential cost and time savings in the design process of components including composite materials.

There are a broad number of examples in literature pertaining to the prediction of residual stress and strain in bi-material geometries. In the simplest example, Timoshenko predicts the curvature and displacement of a one-dimensional bi-material beam using an analytical solution that is driven by the coefficients of thermal expansion and the material stiffness [1]. However, the approach given by Timoshenko is limited to material properties that are uniform and constant. That is not to say the equations proposed by Timoshenko cannot predict the residual stress of a bi-material beam comprised of a thermoset polymer composite reasonably well – it is unable to account for the entire curing process of a composite and important factors, such as polymer shrinkage. Because cure kinetics of a thermoset polymer composite can be quite impactful to the residual stress seen in a composite, White and Hahn developed a process modeling approach for composites [2-3]. The process model follows the temperature history of the composite and follows the transition of a composite from its uncured to cured state. Expanding upon the principles of process modeling of composites, Tavakol et. al. developed a three-dimensional coupled thermomechanical process model that determines the mechanical properties on an element based on the temperature and cure kinetics (i.e. degree of cure) [4]. A similar process was also used by Volk et. al. to predict the residual stresses in an organic matrix composite open hole tension specimen [5]. Full process modeling of thermoset polymer composites often requires many input parameters to fully define the cure kinetics, thermal, and mechanical properties, which may be difficult or costly to obtain. Jumbo et. al. uses an approach that accounts for much of the process modeling by experimentally determining the stress free temperature of epoxy/aluminum and epoxy/steel bi-material strips and isothermally modeling the cooldown of the process from the stress free temperature [6]. Combinations of linear and non-linear material properties in two and three-dimensions were compared to experiments and the analytical solution presented by Timoshenko.

Existing literature shows that residual stress in composites and bi-material entities can be predicted with many different levels of rigor. Therefore, the objective of this study is to determine a simplistic, but effective methodology to predict residual stress in three-dimensional bi-material structures comprised of a thermoset polymer composite and a metal. Specifically, a carbon fiber/epoxy and aluminum bi-material plate and cylinder were simulated with a simplified process that accounts for the coefficients of thermal expansion and polymer shrinkage of the composite similar to that presented by Jumbo et. al. However, as Jumbo et. al. modeled only neat epoxies, the inclusion of a fiber-reinforced composite in the presented work represents an added complexity, which requires consideration of the material's orthotropy. This simulation approach is compared to experiments to determine its viability as an effective methodology to model residual stresses in various geometries.

# 2. PLATE AND CYLINDER EXPERIMENTS

## 2.1 Geometry and Materials

The carbon fiber/epoxy material that was used for this investigation consisted of an 8-harness satin (8HS) weave prepreg with AS4C tows and TCR 3362 resin. Laminates were laid by hand from pre-cut ply kits made using a CNC ply cutter to control geometry and fiber orientation. The fiber volume fraction was approximately 48 % and the material was cured in the form of a bi-material plate or a bi-material cylinder using a standard autoclave process at 176.7 °C.

In both layup configurations, the bi-material plate and cylinder, the composite material was co-bonded to a lightly abraded and acetone cleaned surface of the aluminum. The plate was comprised of a 457.2 mm square, 0.81 mm thick 6061 T-6 aluminum plate with a 406.4 mm square of the composite centered on the aluminum plate. The cylinder was comprised of a 6063 T-6 aluminum cylinder machined to have an outer diameter of 112.3 mm and a thickness of 2.03 mm with the composite placed on the outer diameter of the aluminum cylinder. For both the plate and the cylinder, the composite stack sequence for the plate and cylinder consisted of 4 plies of 8HS weave symmetrically laid up with respect to the mid-thickness plane $[0_2]_s$. This resulted in a composite thickness of approximately 1.6285 mm.

Standard practices of tooling plates, caul plates, release films, bleeder, and edge string bleeder were employed to adequately consolidate and devolatilize the laminate during cure. Edge embedded thermocouples were actively used to monitor and drive the cure of the laminate. A typical in-process view of both configurations can be seen in Figure 1.

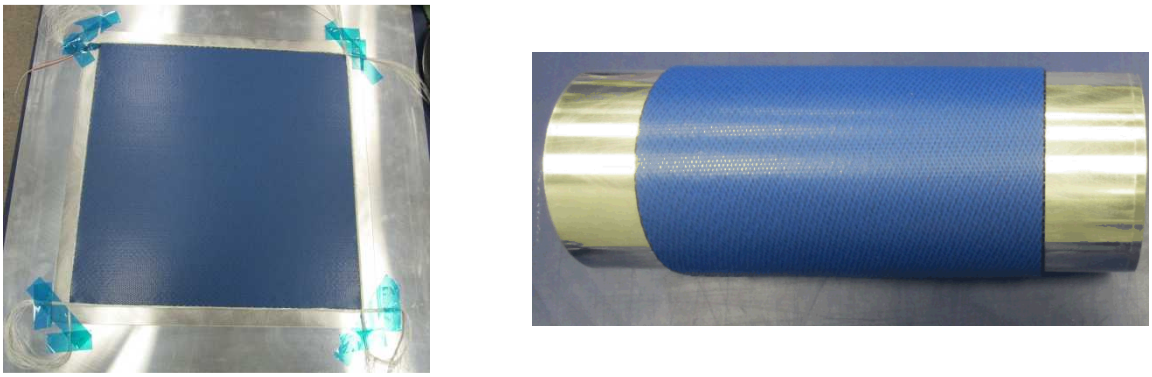

*Figure 1. In-process layup of the bi-material plate (left) and cylinder (right).*

## 2.2 Experimental Procedure and Results

By using a symmetric stack sequence for the composite in both geometries, any thermal residual stress would, in most part, be solely due to the polymer shrinkage and the coefficient of thermal expansion (CTE) mismatch between the aluminum and composite material. The approach in this experimental phase of the investigation was to observe and measure the distortion of both geometric configurations as a function of temperature.

### *2.2.1 Plate*

Knowing the plate would distort with curvature along the diagonal (45° direction) added an additional level of complexity to quantifying the magnitude, as this curvature was not necessarily constant or easily determined. In order to more accurately measure the shape, a Coordinate Measuring Machine (CMM) was used, as shown in Figure 2. The CMM output data points were then used to create a surface model to quantitatively compare with the finite element solution.

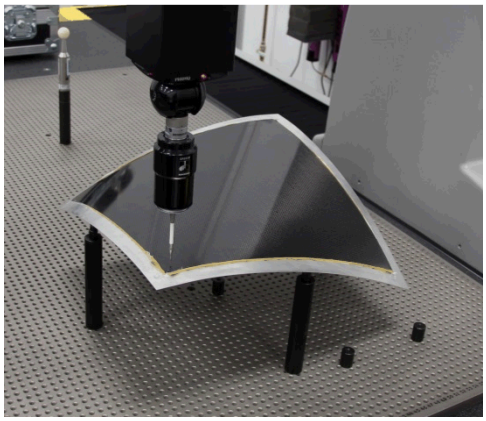

*Figure 2. Distorted bi-material plate being inspected for distortion using CMM.*

With the bi-material plate being distorted at room temperature, the stress-free temperature could then be determined by heating the plate until it became flat. For this, a thermal chamber was programmed to progressively ramp the temperature and dwell at specified intervals attain thermal equilibrium and observe the flatness of the plate. As can be seen in Figure 3, the stress-free temperature appears to be between 140.6 °C and 146.1 °C. Beyond this temperature, the curvature reverses and the composite material is on the concave side.

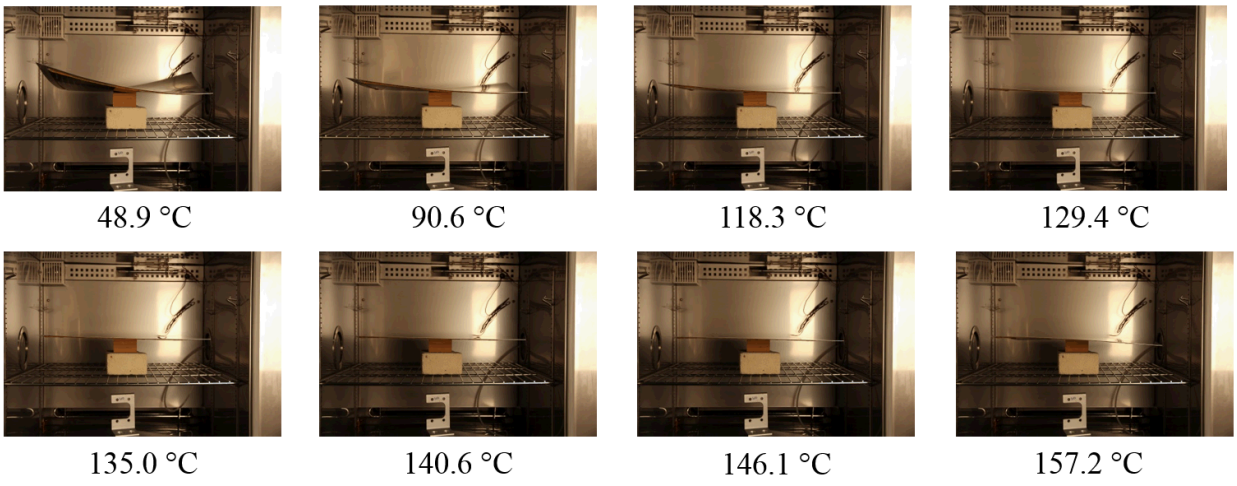


*Figure 3. Bi-material plate distortions at various temperatures.*

### *2.2.2 Cylinder*

The cylinder was machined in order to produce six 25.4 mm wide split rings. The sector removed from each ring to create the split was approximately 35° or 32.5 mm in length, thus allowing the ring to close in on itself due to the residual stress at the interface. The split rings were then progressively heated and cooled in order to quantify the resultant gap as a function of temperature, as shown in Figure 12. The details with the split ring processing can be seen in Figure 4.

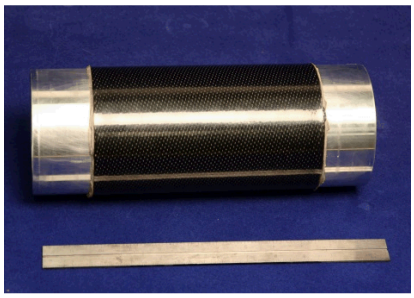

*Consolidated bi-material cylinder*

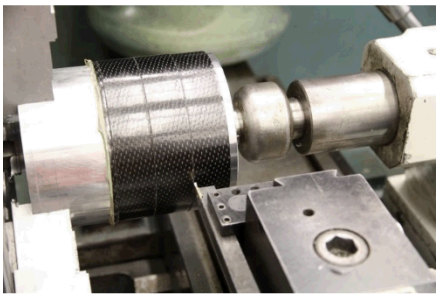

*Lathe cutting cylinder down into rings*

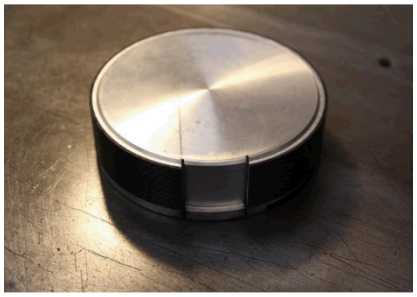

*Ring has been split by removing 35° sector*

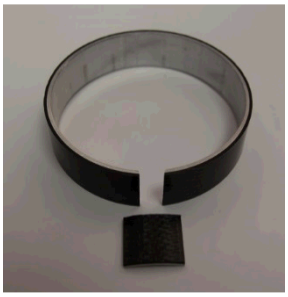

*Ring closes in on itself at room temperature due to residual stresses*

*Figure 4. Bi-material cylinder is processed into split rings to observe the gap width as a function of temperature.*

## 3. COMPUTATIONAL EFFORTS (SIMPLE)

The methodology developed herein provides a simplified method that could be easily applied to more complex geometries without requiring a significant number of experiments (for detailed material properties) or a significant increase in computational cost. As such, it assumes that the residual stress in a bi-material geometry could be reasonably predicted by only taking into account the coefficients of thermal expansion of both materials and the polymer shrinkage of the composite material via the stress free temperature.

### 3.1 Simulation Process

The first step of the simulation isothermally heats the geometries from room temperature (20 °C) to the stress free temperature (143.3 °C) where the simulation is stopped. Heating the geometries to the experimentally determined stress free temperature instead of the cure temperature allows for the effect of polymer shrinkage to be indirectly incorporated. During the curing process, the composite will volumetrically shrink and impart a residual stress in the component. As the geometry begins to cool, the mismatched coefficients of thermal expansion will eventually

nullify the residual stress induced by the polymer shrinkage at the stress free temperature resulting in a stress free temperature that is lower than the cure temperature [7]. By stopping the analysis at the stress free temperature the cured composite material can be activated at a known stress free state for the next analysis step while the aluminum maintains its size and shape. Furthermore, it allows for the deactivation of the un-cured, compliant material properties and the activation of the cured material properties in the subsequent analysis step. This simplifies the simulation of the curing process by simulating the composite material property transformation as a step change.

The second step performs the deactivation of the un-cured composite materials and the activation of the cured composite materials before cooling the geometries back to room temperature. At the onset of the second step the cured composite is activated in a stress free state by only transferring the displacements and temperatures from the initial analysis step. The aluminum, on the other hand, is activated in a fully defined state by transferring stress, strain, and temperature. As the geometries begin to cool, a residual stress will begin to develop due to the dissimilar coefficients of thermal expansion. In the case of the plate, the residual stress warps the plate about a diagonal, and for the cylinder the residual stresses remain undetectable until a sector is removed and spring-in occurs.

### 3.2 Analysis Software

The Sandia National Laboratories' developed implicit finite element code SIERRA Adagio was used to solve the simulations [8]. Adagio is a Lagrangian, three-dimensional implicit code for the finite element analysis of solid structures, which is suitable for the quasistatic nature of these analyses. The cylinder was solved using the default implicit quasistatics settings of Adagio, whereas the plate required implicit dynamics. Implicit dynamics includes the inertial mass and acceleration terms in the equations of motion, whereas they are ignored in implicit quasistatics. Using implicit dynamics and a more realistic time step allowed Adagio to solve the instability of the plate (i.e. warping about either diagonal) more efficiently.

### 3.3 Element Formulation

All simulations were solved using eight-noded hexahedral elements using the uniform gradient (reduced integration) formulation that is default to SIERRA. The strain incrementation was set to be strongly objective rather than the default, midpoint incrementation. Strongly objective incrementations, while computationally more expensive, gives better accuracy for large timesteps and deformations involving both rotation and stretch.

### 3.4 Material Models

The specification of three materials was needed to simulate the curing process of the plate and cylinder: aluminum, un-cured carbon fiber/epoxy composite, and cured carbon fiber/epoxy composite.

Two different aluminum alloys were used in the experiments, 6061-T6 for the plate and 6063-T6 for the cylinder. Both alloys share the same elastic properties; therefore, the same material model, Sierra Adagio's elastic model, was used. The elastic model produces linear elastic behavior for constant (temperature independent) properties and require the specification of the

density, Young's Modulus, and Poisson's ratio, given in Table 1 [8]. The elastic model is sufficient as no yielding or failure was expected to occur in the aluminum.

In its un-cured state, the epoxy matrix of the carbon fiber/epoxy composite has the ability to flow. As such, the un-cured composite was modeled as a compliant and incompressible elastic material using Sierra Adagio's elastic model. Using a perfectly compliant and incompressible material ($E = 0$ and $\nu = 0.5$) resulted in convergence problems that were resolved by using properties sufficiently similar, as shown in Table 1.

The cured carbon fiber/epoxy composite was modeled using Sierra Adagio's elastic orthotropic material model [8]. The regular nine independent constants (Young's modulus, shear modulus, and Poisson's ratios in the three material directions) are needed to fully define the elastic behavior of the cured composite, which were determined through a suite of tension tests or micromechanical modeling. Furthermore, the material model calls for the density and coordinate rotations to properly align the material coordinate system. All properties are described in Table 2.

For the aluminum and cured composite material models, thermal strains were defined using the corresponding coefficients of thermal expansion (CTE). The un-cured composite was given the same CTE as the aluminum to account for the fact that the un-cured composite does not restrict the thermal expansion of the aluminum. The CTE for the aluminum was defined as an average value for a single temperature range, whereas the CTE for the cured composite was defined for two different temperature ranges. The cured composite transitions from the glassy region to the rubbery region (or vice versa) at a temperature of 125.2 °C.

*Table 1. Elastic Material Model Properties.*

| **Material** | **Aluminum 6061/6063[1]** | **Un-Cured Composite** |
|---|---|---|
| Density (kg/m$^3$) | 2,700 | 1,600 |
| Young's Modulus (GPa) | 68.9 | 0.1 |
| Poisson's Ratio | 0.33 | 0.499 |
| CTE (1/K) | 23.4e-06[2] | 23.4e-06 |

[1] [9]
[2] Average value from 20 °C – 100 °C

*Table 2. Elastic Orthotropic Material Model Properties.*

| **Material** | **Cured Composite** | |
|---|---|---|
| | **Glassy Region** | **Rubbery Region** |
| Density (kg/m$^3$) | 1,600 | |
| $E_{11}$ (GPa) | 63.86 | |
| $E_{22}$ (GPa) | 62.74 | |
| $E_{33}$ (GPa) | 8.59 | |
| $\nu_{12}$ | 0.0480 | |
| $\nu_{13}$ | 0.4075 | |
| $\nu_{23}$ | 0.0548 | |
| $G_{12}$ (GPa) | 3.44 | |
| $G_{13}$ (GPa) | 3.27 | |

| $G_{23}$ (GPa) | 3.25 | |
|---|---|---|
| $CTE_{11}$ (1/K) | 3.40e-06 | 1.13e-06 |
| $CTE_{22}$ (1/K) | 3.36e-06 | 1.13e-06 |
| $CTE_{33}$ (1/K) | 7.20e-05 | 2.83e-04 |

## 3.5 Model Geometry

The geometries for the plate and cylinder simulations were generated and meshed in three-dimensions using Cubit. Both simulations were modeled at nominal dimensions and did not take into account any variances during the manufacturing processes. The small dimensional variances would have negligible effect for determining the ability of the modeling method to predict the residual stresses in the plate and cylinder. Furthermore, the composite was modeled as one section with homogenized properties (i.e. each ply was not explicitly modeled).

### *3.5.1 Plate*

The plate was fully modeled (i.e. no symmetry was used). Although the experimental results show symmetry across the diagonal of the plate, a uniform mesh using hexahedral elements cannot be achieved on triangular geometry. The sole boundary condition was applied to the center node of the plate (on the aluminum external surface), which fixed both the displacement and rotation of the node (Figure 2).

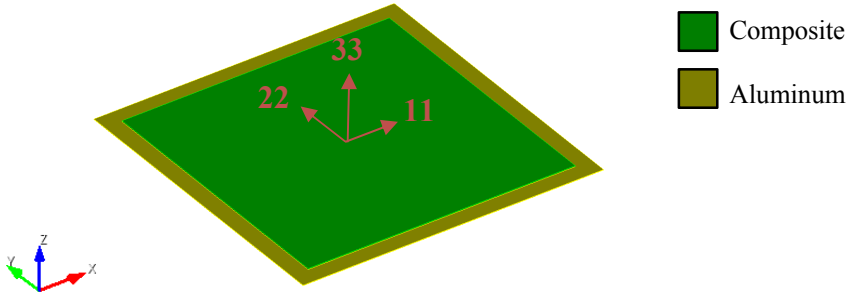


*Figure 5. Bi-material plate simulation geometry.*

### *3.5.2 Cylinder/Split Ring*

The split ring was modeled in quarter symmetry at its final machined state prior to the removal of the sector. Symmetry was specified on the xy and yz planes and a single node was held at zero y-displacement to prevent any motion (Figure 3). While the split ring was manufactured as part of a larger cylinder, the aluminum was expected to remain elastic and, therefore, modeling the split ring in its final state is acceptable. The removed sector was modeled as a separate partition such that it could be easily removed from the model.

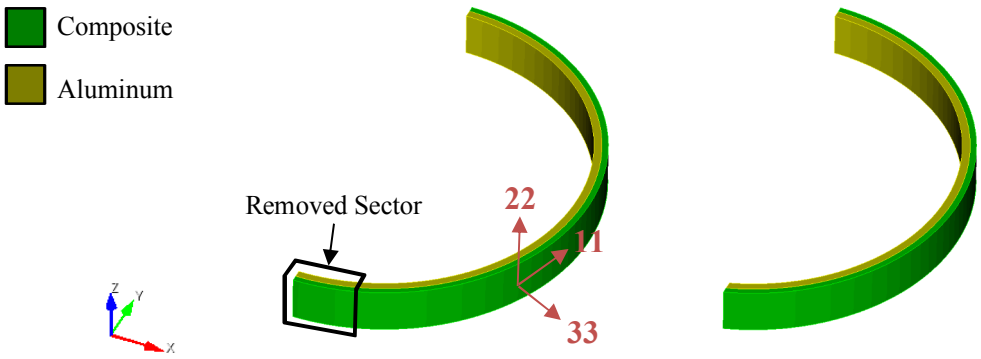


*Figure 6. Bi-material split ring simulation geometry before (left) and after (right) sector removal.*

### 3.6 Mesh Convergence Study

Each model underwent a mesh convergence study in order to verify that the model solution was converging to the same continuum value (maximum displacement for the plate and gap width for the cylinder) regardless of mesh. Additionally, the mesh convergence study aids in determining a balance between computational efficiency and solution error.

The mesh convergence studies followed Richardson's Extrapolation [10]. By using Richardson's Extrapolation, an estimate of the exact value, or the solution corresponding to an element size of zero, can be determined from the solutions to three uniformly refined meshes. The discrete solution, $f$, to a particular mesh can be thought of as the exact (continuum) solution, $f_e$, with the addition of error terms:

$$f = f_e + g_1 h + g_2 h^2 + g_3 h^3 + \cdots \tag{1}$$

From Equation 1 a second order approximation of the exact solution can be made using two different mesh sizes (Equation 2), which then can be generalized for any $p$-th order approximation (Equation 3).

$$f_e = f_1 + \frac{f_1 - f_2}{r^2 - 1} \tag{2}$$

where: $r = h_2/h_1$; ratio of mesh sizes
$f_n$ = discrete solutions

$$f_e = f_1 + \frac{f_1 - f_2}{r^p - 1} \tag{3}$$

The order of convergence, $p$, can be solved using solutions from at least three different meshes:

$$\frac{\varepsilon_{23}}{r_{23}^p - 1} = r_{12}^p \left( \frac{\varepsilon_{12}}{r_{12}^p - 1} \right) \tag{4}$$

where: $r_{12} = h_2/h_1$
$r_{23} = h_3/h_2$
$\varepsilon_{12} = f_1 - f_2$
$\varepsilon_{23} = f_2 - f_3$

Equation 4 can be further simplified if the mesh is scaled by the same factor for each consecutive refinement (i.e. $r_{12} = r_{23}$), as shown by Equation 5:

$$p = \frac{\log(\varepsilon_{23}/\varepsilon_{12})}{\log(r)} \tag{5}$$

The meshes of both the plate and cylinder were scaled by a factor of two in each direction ($r = 2$), which permits the use of the simplified Equation 6 and results in an increase in the total number of elements by a factor of eight for each mesh refinement.

In order to proceed and use the calculated value of $p$ from Equation 6 to estimate the exact solution in Equation 3, the mesh solutions must be confirmed to be within the asymptotic range of convergence. To do this, a grid convergence index (GCI) is calculated for each level of mesh refinement. The GCI gives a percentage value that quantifies how close a solution is to the asymptotic range of convergence. Using the same three solutions from above, two GCIs can be calculated:

$$GCI_{12} = \frac{SF \cdot \left|\frac{f_2 - f_1}{f_1}\right|}{r^p - 1} \;;\; GCI_{23} = \frac{SF \cdot \left|\frac{f_3 - f_2}{f_2}\right|}{r^p - 1} \tag{6}$$

In Equation 6, $SF$ is a safety factor that affects the perception of convergence and has been set to a recommended, conservative value of 3.0. Setting $SF$ equal to 3.0 results in a typical error calculation for second-order methods ($p = 2$) and the mesh is scaled by a factor of 2 ($r = 2$). As the order of convergence increases beyond two, the safety factor undoubtedly becomes more conservative. In order to use $p$ and Equation 2 to estimate the exact solution, the discrete solutions must be verified to reside within the asymptotic range of convergence by satisfying the following:

$$\left(\frac{GCI_{12}}{GCI_{23}}\right) r^p \approx 1 \tag{7}$$

The details of the completed Richardson's Extrapolation for the flat and the cylinder can be found in Table 3 and Table 4 of the subsequent sections, respectively.

### *3.6.1 Plate*

Three meshes were run for the plate, starting with one element through the thickness of each material and progressing to four. The initial mesh (one element through the thickness) was created with an aspect ratio reasonably close to unity (1.30:1.30:1.0). Through uniform mesh refinement, each progressive mesh maintained the same aspect ratio. The finest mesh (four elements through the thickness) resulted in more than five million elements. In order to reduce computational costs and time, only a portion of the plate was modeled for the mesh convergence

study. A 228.6 mm square plate was created with the same mesh sizes, which reduced the number of elements of finest mesh to approximately a quarter of the full plate and significantly reduced the run time. All three of the meshes for the reduced plate were used with Richardson's Extrapolations to estimate the average tip displacement at room temperature to be 29.71 mm. Figure 7 shows the meshes and the error as a function of mesh size for the reduced plate.

*Table 3. Richardson's Extrapolation for the plate model.*

| Simulation | Mesh Size (mm) | Total Elements | Avg. Tip Displacement (mm) | $p$ | $GCI$ | $\left(\frac{GCI_{12}}{GCI_{23}}\right) r^p$ | Predicted Exact Solution (mm) |
|---|---|---|---|---|---|---|---|
| 3 | 1.6285 | 23,328 | 22.6814 | 1.740 | 0.2286<br>0.0650 | 0.9493 | 29.7080 |
| 2 | 0.8143 | 186,624 | 27.6045 | | | | |
| 1 | 0.4071 | 1,492,992 | 29.0783 | | | | |

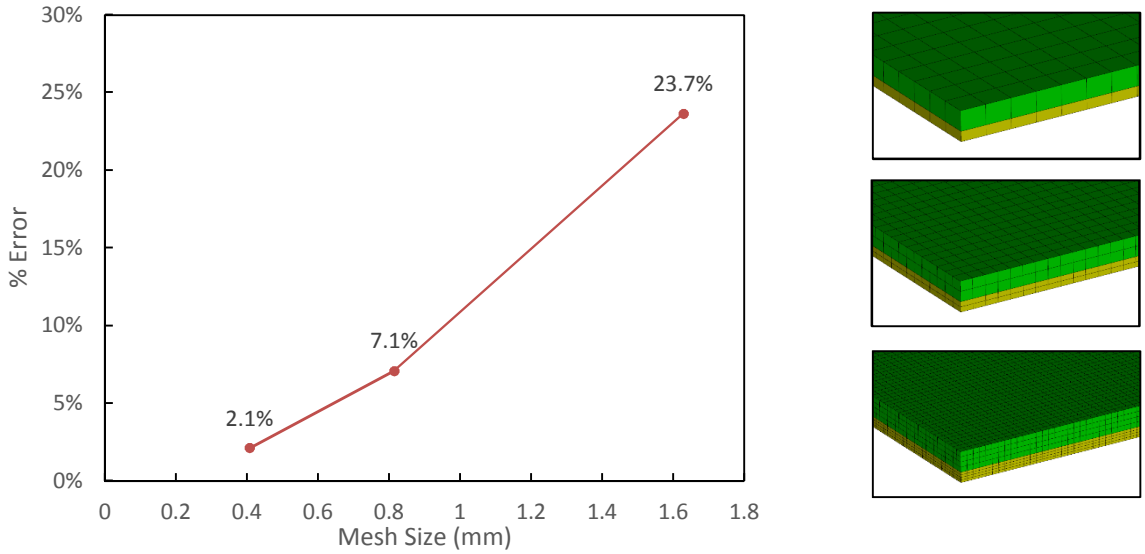


*Figure 7. Error for three mesh sizes of the plate (left) and plate meshes (right): simulation 3 (top), simulation 2 (middle), and simulation 1 (bottom).*

### *3.6.2 Cylinder*

Four meshes were run for the cylinder. As with the plate, the initial mesh started with one element through the thickness of each material, but progressed to eight. The initial mesh of the cylinder was also created with an aspect ratio reasonable close to unity (0.77:0.95:1.0), which was maintained through uniform mesh refinement. The meshes having more than one element through the thickness of each material (Simulations 1-3) were used with Richardson's Extrapolation to estimate the exact cylinder gap at room temperature to be 12.36 mm. Figure 8 shows the meshes for the cylinder model and the predicted gap widths and percent error as a function of mesh size.

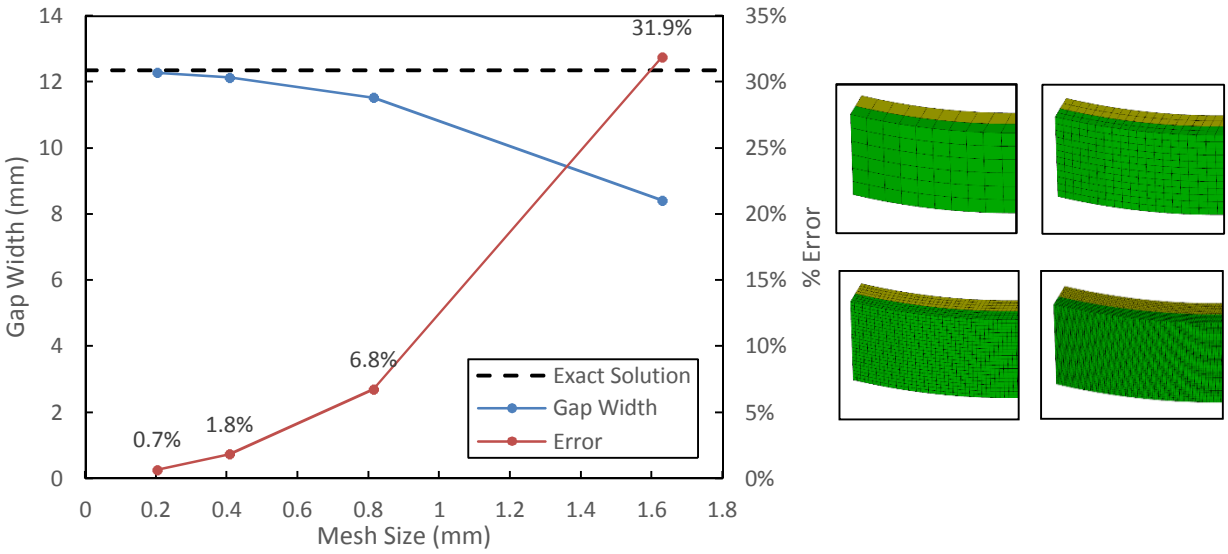


*Figure 8. Gap width and error for four mesh sizes of the split ring (left) and split ring meshes (right): simulation 4 (top, left), simulation 3 (top, right), simulation 2 (bottom, left), and simulation 1 (bottom, right).*

*Table 4. Richardson's Extrapolation for the split ring model.*

| Simulation | Mesh Size (mm) | Total Elements | Gap Width (mm) | $p$ | $GCI$ | $\left(\frac{GCI_{12}}{GCI_{23}}\right) r^p$ | Predicted Exact Solution (mm) |
|---|---|---|---|---|---|---|---|
| 4 | 1.6285 | 1,056 | 8.4220 | | | | |
| 3 | 0.8143 | 8,448 | 11.5254 | 2.074 | 0.0468<br>0.0110 | 0.9882 | 12.3602 |
| 2 | 0.4071 | 67,584 | 12.1334 | | | | |
| 1 | 0.2036 | 540,672 | 12.2778 | | | | |

## 3.7 Results

### *3.7.1 Plate*

The manufactured plate composite surface was measured using a CMM to produce a point cloud representing the plate's displacement, which can be depicted as a surface (Figure 9). The CMM recorded displacements over a 304.8 mm square centered on the plate. The surface of the simulated plate was subtracted from the experimental surface to show the difference between the experiment and simulation in Figure 10.

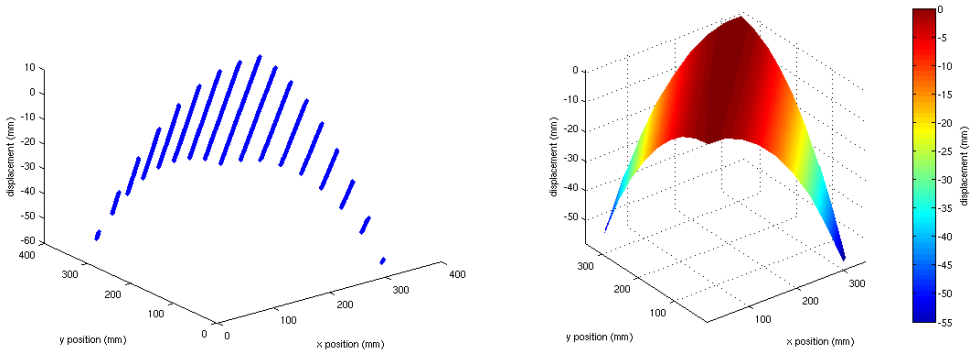


*Figure 9. Plots of the plate experimental point cloud data and associated surface.*

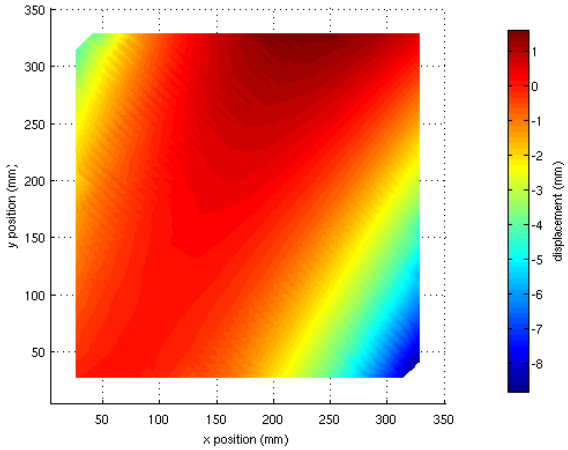


*Figure 10. Difference in displacements between the experiment and simulation.*

### *3.7.2 Cylinder*

As with the manufactured cylinder, the simulated cylinder was reheated after the sector was removed and the gap width was monitored. Figure 11 shows the simulation stress states from Simulation 2 at various times during the process and Figure 12 compares to the experimentally measured gap widths as a function of temperature.

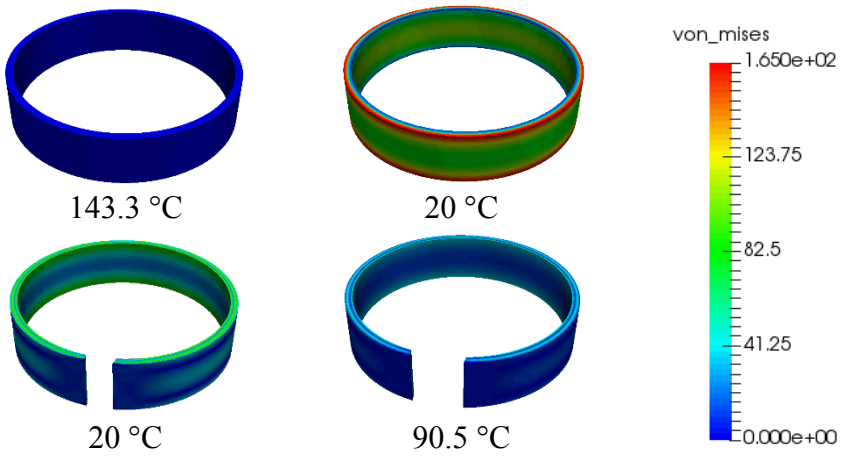


*Figure 11. Cylinder Von Mises Stress (MPa) at various temperatures.*

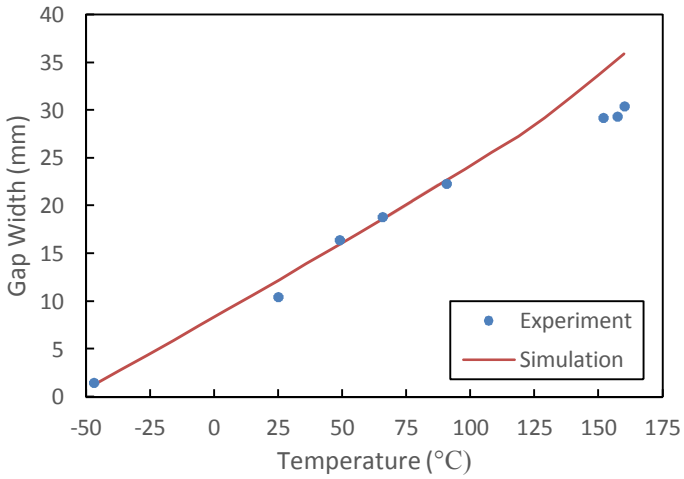


*Figure 12. Comparison of experimental and simulated split ring gap width using the simple method.*

## 4. COMPUTATIONAL EFFORTS (COMPLEX)

The complex methodology performs both a heat transfer and stress analysis in order to specify the composite material properties as a function of location, time, and temperature history. Therefore, unlike the simplified method, the complex method is able to account for effects on non-uniform temperature distributions and degree of cure during the curing process of the composite.

### 4.1 Simulation Process

The processing analysis of the plate and the cylinder was conducted using Abaqus® 6.14-1 finite element software in conjunction with COMPRO®, a process modeling software developed by Convergent Manufacturing Technologies.

The processing of the parts was simulated using a two-step process, which consisted of a heat transfer analysis followed by a stress analysis. In the heat transfer analysis, at each time increment, COMPRO was invoked to calculate the current degree of cure (DOC) of the composite as a function of location, time, and temperature history that the part has experienced. Using the new DOC, the current heat transfer material properties (e.g. thermal conductivity, specific heat, etc.) for the composite were then calculated and used in solving the differential heat transfer equations in Abaqus.

After performing the heat transfer analysis, the temperature fields were read into the stress analysis. Similar to the thermal analysis, COMPRO was invoked to calculate the DOC and associated thermal and mechanical material properties (e.g. modulus, Poisson's ratio, polymer shrinkage coefficient, coefficient of thermal expansion) at each time increment. After the curing step, boundary conditions were applied to the composite parts to prevent undesired rigid body motion, and the parts were allowed to equilibrate to its natural, as-processed configuration.

### 4.2 Results

Figure 13 compares the complex simulation results to the experimentally measured gap widths of the split ring as a function of temperature.

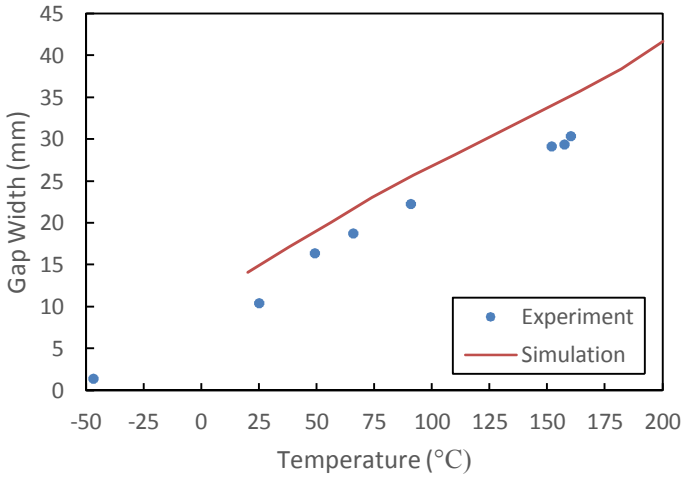


*Figure 13. Comparison of experimental and simulated split ring gap width using the complex method.*

## 5. CONCLUSIONS

A simple and a more complex process modeling methodology were used to predict the residual stresses due to the composite curing process in two different geometries – a bi-material plate and a split ring – and were compared to experimentally determined displacements. The simplistic modeling approach shows good agreement with the experimental deformations of the plate and both modeling approaches show good agreement with the experimental gap widths of the split

ring. The simple model of the plate predicts the displacements within a few millimeters (~10 %) with some error due to the imperfect placement of the plate in the CMM. Both the simple and complex models predict the split ring gap width well below the glass transition temperature (125.2 °C) since majority of the material properties were tested below that temperature. Furthermore, some error in the complex simulation of the split ring can be accounted for due to the fact the TCR 3362 resin was not previously calibrated in COMPRO and properties of another resin were modified such that the glass transition temperature and the elastic properties equaled those of the TCR 3362 resin.

While both methodologies are capable of accurately predicting the residual stress in bi-material geometries containing a composite material, the level of rigor of the complex methodology may not be necessary in certain cases. The simplistic approach of calibrating to an experimentally determined stress free temperature successfully accounts for the polymer shrinkage and, along with the coefficients of thermal expansion, can accurately predict the residual strains with a reduced number of material parameters needed. However, the model does not contain the necessary information to predict other phenomena, such as creep, like the more complex model.

## 6. REFERENCES


1. Timoshenko S. "Analysis of bi-metal thermostats." *Journal of the Optical Society of America* 11(1925):233-255.
2. White, S.R., Hahn, H.T. "Process Modeling of Composite Materials: Residual Stress Development during Cure. Part I. Model Formulation." *Journal of Composite Materials* 26(1992):2402-2422
3. White, S.R., Hahn, H.T. "Process Modeling of Composite Materials: Residual Stress Development during Cure. Part II. Experimental Validation." *Journal of Composite Materials* 26(1992):2423-2453
4. Tavakol, B., Roozbehjavan, R., Ahmed, A., Das, R., Joven, R.m Koushyar, H., Rodriguez, A., Minaie, B. "Prediction of Residual Stresses and Distortion in Carbon Fiber-Epoxy Composite Parts Due to Curing Process Using Finite Element Analysis." *Journal of Applied Polymer Science* (2013):941-950
5. Volk, B.L., Braginsky, M., Hoos, K., Iarve, E., Mollenhauer, D., and Storage, T. "Predicting the open hole tension of organic matrix composites incorporating the effects of processing." *CAMX Conference Proceedings.* Dallas, TX, October 26-29, 2015. *CAMX – The Composites and Advanced Materials Expo* CD-ROM
6. Jumbo, F.S., Ashcroft, I.A., Crocombe, A.D., and Abdel Wahab, M.M. "Thermal residual stress analysis of epoxy bi-material laminates and bonded joints." *International Journal of Adhesion & Adhesives* 30(2010):523-538.
7. Hahn, H.T. "Residual Stresses in Polymer Matrix Composite Laminates." *Journal of Composite Materials* 10(1976):266-278
8. SIERRA SolidMechanics Team (2015). *SIERRA/SolidMechanics 4.38 User's Guide*, Sandia National Laboratories, Albuquerque, NM.

9. Metals Handbook, Vol.2 - Properties and Selection: Nonferrous Alloys and Special-Purpose Materials, ASM International 10th Ed. 1990.
10. Roache, P.J. “Perspective: A Method for Uniform Reporting of Grid Refinement Studies.” *Journal of Fluids Engineering* 116(1994):405-413